PHYSICAL REVIEW A **85**, 013837 (2012)

Magnetic linear birefringence measurements using pulsed fields

P. Berceau,[1] M. Fouché,[1,2,3] R. Battesti,[1] and C. Rizzo[1,*]

[1]*Laboratoire National des Champs Magnétiques Intenses, Unité Propre de Recherche No. 3228 du Centre National de la Recherche Scientifique, Université Paul Sabatier, Université Joseph Fourier, and Institut National des Sciences Appliquées de Toulouse, 31400 Toulouse, France*

[2]*Université de Toulouse, Université Paul Sabatier, Laboratoire Collisions Agrégats Réactivité, Institut de Recherche sur les Systèmes Atomiques et Moléculaires Complexes, F-31062 Toulouse, France*

[3]*Centre National de la Recherche Scientifique, Unité Mixte de Recherche No. 5589, F-31062 Toulouse, France*

(Received 22 September 2011; published 24 January 2012)

In this paper we present the realization of further steps toward the measurement of the magnetic birefringence of a vacuum using pulsed fields. After describing our experiment, we report the calibration of our apparatus using nitrogen gas and discuss the precision of our measurement giving a detailed error budget. Our best present vacuum upper limit is $\Delta n \leqslant 5.0 \times 10^{-20}$ T^{-2} per 4 ms acquisition time. We finally discuss the improvements necessary to reach our final goal.

DOI: 10.1103/PhysRevA.85.013837 PACS number(s): 42.25.Lc, 78.20.Ls, 12.20.−m

I. INTRODUCTION

Experiments on the propagation of light in a transverse magnetic field date from the beginning of the 20th century. Kerr [1] and Majorana [2] discovered that linearly polarized light, propagating in a medium in the presence of a transverse magnetic field, acquires an ellipticity. In the following years, this linear magnetic birefringence was studied in detail by Cotton and Mouton [3] and it is known nowadays as the Cotton-Mouton effect. It corresponds to an index of refraction $n_\parallel$ for light polarized parallel to the magnetic field B, which is different from the index of refraction $n_\perp$ for light polarized perpendicular to the magnetic field. For symmetry reasons, the difference between $n_\parallel$ and $n_\perp$ is proportional to B^2. Thus, an incident linearly polarized light exits from the magnetic-field region elliptically polarized. For a uniform B over an optical path L, the ellipticity is given by

$$\Psi = \pi \frac{L}{\lambda} \Delta n B^2 \sin 2\theta, \tag{1}$$

where λ is the wavelength of light in vacuum, $\Delta n = n_\parallel - n_\perp$ at $B = 1$ T, and θ is the angle between light polarization and the magnetic field.

The Cotton-Mouton effect exists in any medium and quantum electrodynamics predicts that magnetic linear birefringence exists also in vacuum, which has been shown [4,5] as a result of the effective Lagrangian established by Kochel, Euler, and Heisenberg [6,7]. At the lowers two orders in α, the fine-structure constant Δn can be written (in units of T^{-2}) as

$$\Delta n = \frac{2}{15} \frac{\alpha^2 \hbar^3}{m_e^4 c^5 \mu_0} \left(1 + \frac{25}{4\pi}\alpha\right), \tag{2}$$

where $\hbar$ is the Planck constant over 2π, m_e is the electron mass, c is the speed of light in vacuum, and μ_0 is the magnetic constant. The term α^2 is given in Ref. [4]. The term α^3 was reported in Ref. [8] and corresponds to the lowest-order radiative correction. Its value is about 1.5% of the α^2 term. Using the CODATA recommended values for the fundamental constants [9], Eq. (2) gives $\Delta n = (4.031\,699 \pm 0.000\,002) \times 10^{-24}$ T^{-2}.

As we see, the error due to the uncertainty of fundamental constants is negligible compared to the error coming from the fact that only the first-order QED radiative correction has been calculated. The QED α^4 radiative correction should affect the fourth digit and the QED α^5 radiative correction the sixth digit. Thus, a measurement of Δn up to a precision of a few parts per 10^6 (ppm) remains a pure QED test.

Experimentally, the measurement of the Cotton-Mouton effect is usually very challenging, especially in dilute matter, thus all the more so in vacuum. Several groups have attempted to observe vacuum magnetic birefringence [10,11], but this very fundamental prediction still has not been experimentally confirmed.

Gas measurements date back to the late 1930s [12] and the first systematic work of Buckingham *et al.* was published in 1967 [13]. Investigations concerned benzene, hydrogen, nitrogen, nitrogen monoxide, and oxygen at high pressures as well as ethane. Since then, many more papers concerning the effect in gases have been published and Cotton-Mouton effect experiments have been employed as sensitive probes of the electromagnetic properties of molecules [12].

The measurement of the Cotton-Mouton effect in gases is not only important to test quantum chemical predictions. It is a crucial test for any apparatus that is dedicated to the search for vacuum magnetic birefringence. Measurement of the Cotton-Mouton effect in a gas is a milestone in the improvement of the sensitivity of such an apparatus. Typically measurements of the linear magnetic birefringence in nitrogen gas are used to calibrate a setup [10,11,14].

In the following we present magnetic linear birefringence measurements performed in the framework of our *biréfringence magnétique du vide* (BMV) project. It is based on the use of strong pulsed magnetic fields, which is different compared to other experiments searching for vacuum magnetic birefringence, and on a very high finesse Fabry-Pérot cavity to increase the effect to be measured by trapping the light in the magnetic-field region. The use of pulsed fields for such measurements was proposed in Ref. [15]. In principle, pulsed magnetic fields can be as high as several tens of teslas,

---

[*] carlo.rizzo@lncmi.cnrs.fr

which increases the signal, and they are rapidly modulated, which decreases the $1/f$-flicker noise resulting in an increase of the signal-to-noise ratio. Both advantages are supposed to compensate for the loss of duty cycle since only a few pulses per hour are possible. A feasibility study, which discusses most of the technical issues related to the use of pulsed fields coupled to precision optics for magnetic linear birefringence measurements, can be found in Ref. [16].

In this paper we present the realization of further steps toward the measurement of the magnetic birefringence of the vacuum using pulsed fields. After describing our BMV experiment, we report the calibration of our apparatus with nitrogen gas and discuss the precision of our measurement, giving a detailed error budget. Finally, the present vacuum upper limit is reported and we discuss the perspectives to reach our final goal.

II. EXPERIMENTAL SETUP AND SIGNAL ANALYSIS

A. Apparatus

The BMV experiment is detailed in Ref. [16]. Briefly, as shown in Fig. 1, 30 mW of a linearly polarized Nd:YAG laser beam ($\lambda = 1064$ nm) is injected into a Fabry-Pérot cavity consisting of the mirrors M_1 and M_2. The laser frequency is locked to the cavity resonance frequency using the Pound-Drever-Hall method [17]. To this end, the laser is phase modulated at 10 MHz with an electro-optic modulator. The beam reflected by the cavity is then detected by the photodiode Ph_r. This signal is used to drive the acousto-optic modulator (AOM) frequency for a fast control and the Peltier element of the laser for a slow control of the laser frequency.

Our birefringence measurement is based on an ellipticity measurement. Light is polarized just before entering the cavity by polarizer P. The beam transmitted by the cavity is then analyzed by analyzer A crossed at maximum extinction and collected by a low-noise photodiode Ph_e (the intensity of the extraordinary beam I_e). The analyzer also has an escape window that allows us to extract the ordinary beam (intensity I_t), which corresponds to the polarization parallel to P. This beam is collected by the photodiode Ph_t.

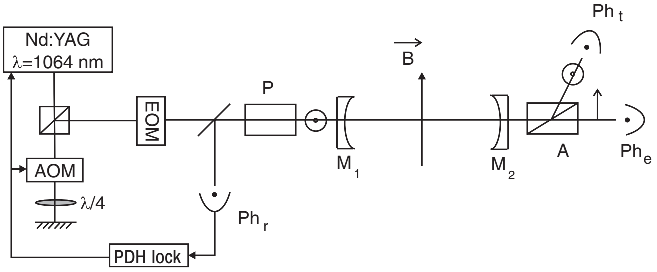

FIG. 1. Experimental setup. A Nd:YAG laser is frequency locked to the Fabry-Pérot cavity consisting of mirrors M_1 and M_2. The laser beam is linearly polarized by polarizer P and analyzed with polarizer A. This analyzer allows one to extract the extraordinary beam sent on photodiode Ph_e as well as the ordinary beam sent on photodiode Ph_t. The beam reflected by the cavity analyzed on the photodiode Ph_r is used for the cavity locking. A transverse magnetic field B can be applied inside the cavity in order to study the magnetic birefringence of the medium. The following denotations are used: EOM, electro-optic modulator; AOM, acousto-optic modulator; and PDH, Pound-Drever-Hall.

All the optical components from polarizer P to analyzer A are placed in an ultrahigh-vacuum chamber. In order to perform birefringence measurements on high-purity gases, the vacuum chamber is connected to several gas bottles through leak valves that allow one to precisely control the amount of injected gas. Finally, since the goal of the experiment is to measure magnetic birefringence, magnets surround the vacuum pipe. The transverse magnetic field is created due to pulsed coils described in Ref. [18] and briefly detailed in the following section.

Both signals collected by the photodiodes outside the cavity are simultaneously used in the data analysis as follows:

$$\frac{I_e}{I_t} = \sigma^2 + \Psi_{\mathrm{tot}}^2, \tag{3}$$

where Ψ_{tot} is the total ellipticity acquired by the beam going from P to A and σ^2 is the polarizer extinction ratio. Our polarizers are Glan laser prisms, which have an extinction ratio of 2×10^{-7}.

The origin of the total ellipticity of the cavity is due to the intrinsic birefringence of mirrors M_1 and M_2, as will be discussed in Sec. II C 2. We define the ellipticity imparted to the linearly polarized laser beam when light passes through each mirror substrate as $\Gamma_{s1,2}$ and the one induced by the reflecting layers of the mirrors as Γ_c. An additional component Ψ of the total ellipticity can be induced by the external magnetic field. Since we use pulsed magnetic fields, this ellipticity is a function of time. Finally, if the ellipticities are small compared to unity, one gets

$$\frac{I_e(t)}{I_t(t)} = \sigma^2 + [\Gamma + \Psi(t)]^2, \tag{4}$$

where $\Gamma = \Gamma_{s1} + \Gamma_{s2} + \Gamma_c$ is the total static birefringence.

B. Magnetic field

It is clear from Eq. (1) that one of the critical parameter for experiments looking for magnetic birefringence is B^2L. Our choice has been to reach a B^2L as high as possible while having a B as high as possible with an L such as to set up a tabletop low-noise optical experiment. This is fulfilled using pulsed magnets that can provide fields of several tens of teslas. Our apparatus consists of two magnets, called X-coils. The principle of these magnets and their properties are described in detail in Refs. [16,18].

The magnetic-field profile along the longitudinal z axis, which corresponds to the axis of propagation of the light beam, has been measured with a calibrated pickup coil. Figure 2 shows the normalized profile of an X-coil. The magnetic field is not uniform along z. We define B_{max} as the maximum field provided by the coil at its center and L_B as the equivalent length of a magnet producing a uniform magnetic field B_{max} such that

$$\int_{-\infty}^{+\infty} B^2(z)dz = B_{\mathrm{max}}^2 L_B, \tag{5}$$

where L_B is about the half of the X-coil's length. Each X-coil currently used has reached more than 14 T over 0.13 m of

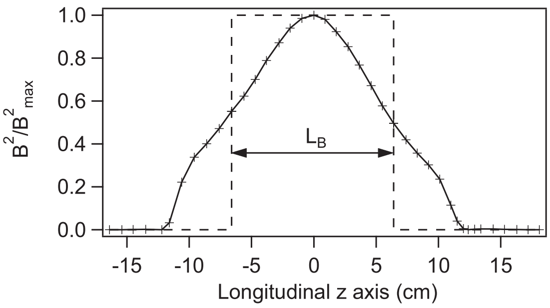

FIG. 2. Normalized profile of the square of the magnetic field along the longitudinal $z$axis (solid line) inside one X-coil. This is compared to the equivalent uniform magnetic field (dashed line) over the effective magnetic length L_B (see the text).

effective length corresponding to 25 T^2 m. The total duration of a pulse is a few milliseconds. The magnetic field reaches its maximum value within 2 ms.

The pulsed coils are immersed in a liquid-nitrogen cryostat to limit the consequences of heating, which could be a cause of permanent damage to the coil's copper wire. The pulse duration is short enough that the coil, starting at liquid-nitrogen temperature, always remains at a safe level i.e., below room temperature. A pause between two pulses is necessary to let the magnet cool down to the equilibrium temperature, which is monitored via the X-coils' resistance. The maximum repetition rate is 5 pulses per hour.

C. Fabry-Pérot cavity

The other key point of our experiment is to accumulate the effect due to the magnetic field by trapping the light between two ultrahigh-reflectivity mirrors constituting a Fabry-Pérot cavity. Its length has to be large enough to leave a wide space so as to insert our two cylindrical cryostats (with a diameter of 60 cm for each cryostat) and vacuum pumping system. The length of the cavity is $L_c = 2.27$ m, which corresponds to a free spectral range of $\Delta^{\mathrm{FSR}} = c/2nL_c \simeq 66$ MHz, with n the index of refraction of the considered medium in which the cavity is immersed. This index of refraction can be considered equal to one. The total acquired ellipticity Ψ is linked to the ellipticity ψ acquired in the absence of a cavity and depends on the cavity finesse F as follows [19]:

$$\Psi = \frac{2F}{\pi}\psi, \tag{6}$$

where F is given by

$$F = \frac{\pi\sqrt{R_M}}{1 - R_M}, \tag{7}$$

with R_M the intensity reflection coefficient, which is supposed to be the same for both mirrors. A finesse as high as possible is essential to increase the induced signal.

1. *Cavity finesse and transmission*

Experimentally, the finesse is inferred from a measurement of the photon lifetime τ inside the cavity as presented in Fig 3. For $t < t_0$, the laser is locked to the cavity. The laser intensity is then switched off at t_0 due to the AOM shown in Fig. 1 and used as an ultrafast commutator. For $t > t_0$, one sees the typical exponential decay of the intensity of the transmitted ordinary beam [20]

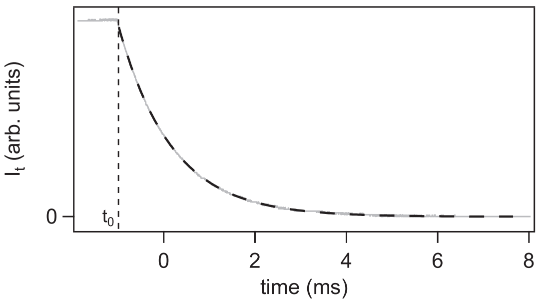

FIG. 3. Time evolution of the intensity of the ordinary beam (gray solid line). The laser is switched off at $t = t_0$. Experimental data are fitted by an exponential decay (black dashed line), giving a photon lifetime of $\tau = 1.16$ ms, a finesse of $F = 481\,000$, and a linewidth of $\Delta\nu = c/2nL_cF = 137$ Hz.

$$I_t(t) = I_t(t_0)e^{-(t-t_0)/\tau}. \tag{8}$$

The photon lifetime is related to the finesse of the cavity through the relation

$$\tau = \frac{nL_cF}{\pi c}. \tag{9}$$

By fitting our data with Eq. (8) we get $\tau = 1.16$ ms, which corresponds to a finesse of $F = 481\,000$ and a cavity linewidth of $\Delta\nu = c/2nL_cF = 137$ Hz. We summarize in Table I the performances of some well-known sharp cavities at $\lambda = 1064$ nm, showing the quality of our cavity.

The transmission of the cavity T_c is another important parameter. It corresponds to the intensity transmitted by the cavity divided by the intensity incident on the cavity when the laser frequency is locked. Indeed, in order not to be limited by the noise of photodiodes Ph_t and Ph_e, I_t and I_e have to be sufficiently high. This point is particularly critical for I_e, which corresponds to the intensity transmitted by the cavity multiplied by σ^2. With a Ph_e noise equivalent power of 11 $\mathrm{fW}/\sqrt{\mathrm{Hz}}$, we need an incident power greater than 0.2 nW so as not to be limited by the electronic noise of Ph_e.

Our cavity transmission is 20%. The measurements of the finesse and the transmission allow us to calculate mirrors properties such as their intensity transmission T_M and their losses P_M as a result of the following relations:

$$F = \frac{\pi}{T_M + P_M}, \tag{10}$$

$$T_c = \left(\frac{T_M F}{\pi}\right)^2, \tag{11}$$

supposing that the mirrors are identical. We found $T_M = 3$ ppm and $P_M = 3.5$ ppm, which correspond to the specifications provided by the manufacturer.

To conclude, our high-finesse cavity enhances the Cotton-Mouton effect by a factor $2F/\pi = 306\,000$ and its transmission allows measurements that are not limited by the noise of the detection photodiodes.

TABLE I. Performance summary of the sharpest infrared interferometers in the world. The following denotations are use: L_c is the length of the Fabry-Pérot cavity, Δ^{FSR} is its full spectral range, F is the cavity finesse, τ is the photon lifetime, $\Delta\nu$ is the frequency linewidth, and $Q = \nu_{\mathrm{laser}}/\Delta\nu$ is the quality factor of the interferometer, with ν_{laser} the laser frequency.

Interferometer	Ref.	L_c(m)	Δ^{FSR} (kHz)	F	τ (μs)	$\Delta\nu$ (Hz)	Q
VIRGO	[21]	3000	50	50	160	1000	2.8×10^{11}
TAMA300	[22]	300	500	500	160	1000	2.8×10^{11}
PVLAS	[11]	6.4	23 400	70 000	475	335	8.4×10^{11}
LIGO	[23]	4000	37	230	975	163	17×10^{11}
BMV	this work	2.27	66 000	481 000	1160	137	21×10^{11}

2. *Cavity birefringence*

The origin of the total static ellipticity is due to the mirror intrinsic phase retardation. Mirrors can be regarded as wave plates and for small birefringence, the combination of both wave plates gives a single wave plate. The phase retardation and the axis orientation of this equivalent wave plate depend on the birefringence of each mirror and on their respective orientations [19,24].

The intrinsic phase retardation of the mirrors is a source of noise limiting the sensitivity of the apparatus. Moreover, since our signal detection corresponds to a homodyne technique, the static ellipticity Γ is used as a zero-frequency carrier. To reach a shot-noise-limited sensitivity, one needs Γ to be as small as possible [16], implying that the phase retardation axes of both mirrors have to be aligned. For magnetic birefringence measurements, both mirrors' orientation is adjusted in order to have $10^{-3} < \Gamma < 3 \times 10^{-3}$ rad.

The measurement of the total ellipticity as a function of mirror orientation allows us to calculate the mirror intrinsic phase retardation per reflection. The experimental procedure is presented in Ref. [25]. The deduced phase retardation for our mirrors is $\delta_M = (7 \pm 6) \times 10^{-7}$ rad. Although the origin of the mirrors' static birefringence is still unknown, a review of the existing data shows that for interferential mirrors, the phase retardation per reflection decreases when reflectivity increases [25]. This observation is confirmed by our present measurement. It is also in agrement with the empirical trend given in Ref. [25]: $\delta_M \simeq 0.1(1 - R_M)$. Numerical calculations show that this trend can be explained by assuming that the effect is essentially due to the layers close to the substrate.

As previously stated, mirror birefringence has two contributions: One comes from the substrate and the other is due to the reflecting layers. Whereas previous measurements do not allow one to distinguish between the two contributions, we will see that this can be achieved with the measurement of I_e decay.

A typical time evolution of I_e when the incident beam locked to the cavity is switched off is shown in Fig. 4. We see that this curve cannot be fitted by an exponential decay. As explained in Ref. [26], one has to take into account the intrinsic birefringence of the cavity. Nevertheless, the expression derived in Ref. [26], which takes into account only the reflecting layer's birefringence, does not always fit our data. The evolution of I_e sometimes presents an unexpected behavior: Whereas photons no longer enter the cavity at $t = t_0$, the extraordinary intensity starts growing before decreasing. To reproduce this behavior, one has to take into account the substrate birefringence.

We now calculate the transmitted intensity along the round-trip inside the cavity.

For $t \leqslant t_0$, the laser is continuously locked to the cavity. According to Eq. (4), the intensities of the ordinary and extraordinary beams are related by

$$I_e(t \leqslant t_0) = [\sigma^2 + (\Gamma_{s2} + \Gamma_{s1} + \Gamma_c)^2] I_t(t \leqslant t_0). \quad (12)$$

At $t = t_0$, the laser beam is abruptly switched off and the cavity empties gradually. The ordinary and extraordinary beams are slightly transmitted at each reflection on the mirrors; however, because these mirrors are birefringent, some photons of the ordinary beam are converted into the extraordinary one. The reverse effect is neglected because $I_e \ll I_t$.

We then follow the same procedure as in Ref. [26] to calculate the time evolution of I_e. For $t > t_0$, one gets

$$I_e(t) = I_t(t) \left\{ \sigma^2 + \left[\Gamma_{s1} + \Gamma_{s2} + \Gamma_c \left(1 + \frac{t - t_0}{2\tau} \right) \right]^2 \right\}. \quad (13)$$

The behavior shown in Fig. 4 is reproduced if $\Gamma_{s1} + \Gamma_{s2} \simeq -\Gamma_c$. This expression is used to fit our experimental data plotted in Fig. 4. We find a photon lifetime of $\tau = 960$ μs, which is in good agreement when fitting I_t [27], $\Gamma_{s1} + \Gamma_{s2} = 2 \times 10^{-3}$ rad, and $\Gamma_c = -7 \times 10^{-3}$ rad. We have evidence that the substrate is birefringent and that this birefringence contributes to the total ellipticity due to the cavity.

D. Signal analysis

The voltage signals V_e and V_t provided by Ph$_e$ and Ph$_t$ are the starting point of our analysis. Voltage signals have to

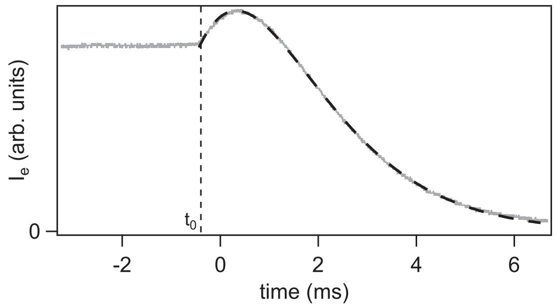

FIG. 4. Time evolution of the intensity of the extraordinary beam (gray solid line). The laser is switched off at $t = t_0$. Experimental data are perfectly fitted by Eq. (13) (black dashed line).

be converted into intensity signals by using the photodiode conversion factors g_e and g_t:

$$I_e = g_e V_e, \tag{14}$$

$$I_t = g_t V_t. \tag{15}$$

As demonstrated in Ref. [26], before analyzing raw signals one has to take into account the first-order low-pass filtering of the cavity. In Fourier space $I_{t,\mathrm{filtered}}$ is given by

$$I_{t,\mathrm{filtered}}(\omega) = \frac{1}{1 + i\frac{\omega}{\omega_c}} I_t(\omega), \tag{16}$$

where $\nu_c = \omega_c/2\pi = 1/4\pi\tau$ is the cavity cutoff frequency. Then, according to Eq. (4), the ellipticity $\Psi(t)$ to be measured can be written as

$$\Psi(t) = -\Gamma + \sqrt{\frac{I_e(t)}{I_{t,\mathrm{filtered}}(t)} - \sigma^2}. \tag{17}$$

The total static birefringence Γ is measured a few milliseconds just before the beginning of the magnetic pulse, thus when $\Psi(t) = 0$.

In contrast, Ψ is proportional to the square of the magnetic field and thus can be written as

$$\Psi(t) = \kappa B^2_{\mathrm{filtered}}(t). \tag{18}$$

Since the photon lifetime is comparable with the rise time of the magnetic field, the first-order low-pass filtering of the cavity also has to be taken into account for the quantity $B^2(t)$ as in Ref. [26]. To recover the value of the constant κ we calculate for each pulse the correlation between $\Psi(t)$ and $B^2_{\mathrm{filtered}}(t)$:

$$\kappa = \frac{\int_0^{T_i} \Psi(t) B(t)^2_{\mathrm{filtered}} dt}{\int_0^{T_i} [B(t)^2_{\mathrm{filtered}}]^2 dt}, \tag{19}$$

where T_i is the integration time. A statistical analysis gives the mean value of κ and its uncertainty.

The magnetic birefringence Δn is finally given by

$$\Delta n(T,P) = \frac{\kappa}{4\pi\tau\Delta^{\mathrm{FSR}}} \frac{\lambda}{L_B} \frac{1}{\sin 2\theta} \tag{20}$$

and Δn is thus expressed in T^{-2}. The terms T and P correspond to the gas temperature and pressure when measurements of magnetic birefringence on gases are performed. We define the normalized birefringence Δn_u as Δn for $P = 1$ atm and $B = 1$ T.

III. EXPERIMENTAL PARAMETERS AND ERROR BUDGET

In the following, to evaluate the precision of our apparatus in the present version, we list the uncertainties at 1σ on the measurement of the parameters of Eq. (20) as recommended in Ref. [28]. The uncertainty of the magnetic birefringence has two origins. The evaluation of the uncertainty by a statistical analysis of a series of observations is termed a type-A evaluation and mainly concerns the measurement of τ and κ. An evaluation by means other than the statistical analysis of a series of observations, calibrations for instance, is termed a type-B evaluation and especially affects the parameters B, Δ^{FSR}, L_B, λ, and θ.

A. Photon lifetime in the Fabry-Pérot cavity

The photon lifetime τ is measured by analyzing the exponential decay of the intensity of the transmitted light. Several measurements have been performed both before and after almost each magnetic pulse. The uncertainty of the value of τ comes from the fact that mirrors can move slightly because of thermal fluctuations and acoustic vibrations. Measurements conducted under the same experimental conditions have been studied statistically, leading to a relative variation of τ that does not exceed 2 at the 1σ level. Data taken during the operation, i.e., before and after magnetic pulses, show the same statistical properties as the ones taken without any magnetic field. Thus, the magnetic field does not cause additional change in τ.

B. Correlation factor

The correlation factor κ is given by Eq. (19). The type-A uncertainty of κ depends on the measurement of Ψ and thus on the experimental parameters given in Eq. (17). In practice, we pulse the magnets several times in the same experimental conditions to obtain a set of values of κ. The distribution of the κ values is found to be Gaussian and we assume that its standard deviation corresponds to the type-A uncertainty of κ. For our measurements performed with nitrogen and presented in Sec. IV B, the type-A relative uncertainty is typically 3.5%. The standard uncertainty of the average value of κ can then be reduced, thus increasing the number of pulses.

Type-B uncertainties depend on those of the square of the magnetic field, the photodiode conversion factors, and the filter function applied to the field. To measure the magnetic field during operation, we measure the current that is injected in our X-coil. As mentioned in Ref. [18], the form factor B/I has been determined experimentally during the test phase by varying the current inside the X-coil (modulated at room temperature or pulsed at liquid-nitrogen temperature) and by measuring the magnetic field induced on a calibrated pickup coil. These measurements have led to a relative type-B uncertainty of $\delta B/B = 0.7\%$ for the magnetic field corresponding to a type-B uncertainty of κ of 1.4%.

The ratio g_e/g_t is measured from time to time by sending the same light intensities to each photodiode. The relative uncertainty in this parameter is 1.5%, which corresponds to the same amount of relative uncertainty in κ.

The terms $I_t(t)$ and $B^2(t)$ are also filtered by a function that involves the parameter τ. We have empirically determined that a τ variation of 2% led to a κ variation of 0.8%. We can finally add quadratically the uncertainties above and deduce that a type-B uncertainty of 2.2% must be taken into account for every measurement of the correlation factor κ.

C. Frequency splitting between perpendicular polarizations

In this section we evaluate the attenuation of the extraordinary beam transmitted by our sharp resonant Fabry-Pérot cavity on which the laser's ordinary beam is frequency locked. Let us suppose that the ordinary (extraordinary) beam resonates in the interferometer at the frequency ν_t (ν_e). The laser is locked to the cavity due to the ordinary beam. Thus ν_t

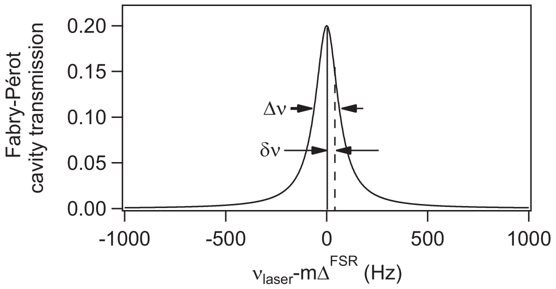

FIG. 5. Airy function of our Fabry-Pérot cavity (with a linewidth of $\Delta\nu$ = 137 Hz, a transmission of $T_c = 20\%$, and where m is an integer). The frequency of the ordinary beam is assumed to be locked at the top of the transmission function (solid line) and the frequency ν_e of the extraordinary beam is shifted from ν_t by a quantity $\delta\nu$ (dashed line).

corresponds to the top of the transmission Airy function A of the Fabry-Pérot cavity, which is given by

$$A(\nu) = \frac{T_c}{1 + \frac{4F^2}{\pi^2}\sin^2\left(\frac{2\pi n L_c}{c}\nu\right)}. \tag{21}$$

The frequency ν_e is shifted from ν_t by a quantity $\delta\nu$, as shown in Fig. 5. The frequency splitting $\delta\nu = \nu_t - \nu_e$ can be expressed as a function of the phase retardation δ acquired along a round-trip between the ordinary and extraordinary beams:

$$\delta\nu = \frac{c}{2\pi n L_c}\delta = \frac{F\Delta\nu}{\pi}\delta. \tag{22}$$

This formula indicates that in order to have a splitting that is very small compared to the cavity linewidth ($\delta\nu \ll \Delta\nu$), the phase retardation δ must satisfy the following condition:

$$\delta \ll \frac{\pi}{F}, \tag{23}$$

which is equivalent to the condition on the acquired total ellipticity Ψ:

$$\Psi \ll 1. \tag{24}$$

By combining Eqs. (21) and (22), we obtain the factor of attenuation a of the transmitted extraordinary beam's intensity given by

$$\begin{aligned} a = \frac{A(\nu_e)}{A(\nu_t)} &= \frac{1}{1 + \frac{4F^2}{\pi^2}\sin^2\left(\frac{2\pi n L_c}{c}\delta\nu\right)} \\ &= \frac{1}{1 + \frac{4F^2}{\pi^2}\sin^2(\delta)}. \end{aligned} \tag{25}$$

The attenuation factor a is plotted as a function of δ in Fig. 6 for a finesse $F = 481\,000$. The *real* intensity I_e of the extraordinary beam transmitted by the cavity is obtained from the corrected *measured* intensity I_e^{meas} as $I_e = I_e^{\mathrm{meas}}/a$.

First, the frequency splitting can be due to our birefringent cavity. As in Ref. [19], we consider both cavity mirrors to be equivalent to a single wave plate with phase retardation $\delta_w = \delta$ between both polarizations. The total phase retardation δ_w is

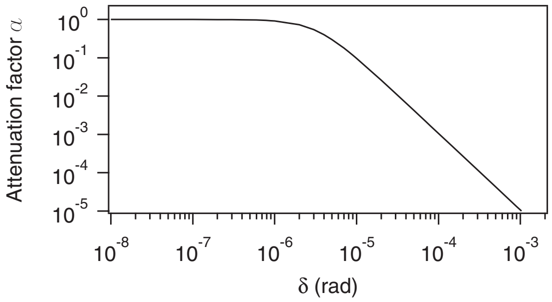

FIG. 6. Attenuation factor a as a function of the phase retardation δ between both polarizations.

linked to the cavity mirrors' $M_1$and M_2own phase retardation δ_1 and δ_2 as [19]

$$\delta_w = \sqrt{(\delta_1 - \delta_2)^2 + 4\delta_1\delta_2\cos^2(\theta_m)}. \tag{26}$$

To set a δ_w as small as possible so as to minimize the correction to I_e^{meas}, one needs to adjust the angle θ_m between the neutral axes of both mirrors. This way, we set a δ_w of the order of a few 10^{-8} rad, corresponding to a correction smaller than 0.001% on I_e^{meas}.

Second, the frequency splitting between both polarizations can be due to the induced magnetic birefringence of the medium inside the chamber. As seen above, the induced ellipticity given by Eq. (24) must be well below 1 rad. This condition is always satisfied in the range of pressure and field we are working. The induced ellipticity does not exceed 10^{-2} rad. This corresponds at worst to a phase retardation of $\delta = 10^{-7}$ rad. The attenuation factor I_e^{meas} is thus smaller than 0.1%.

In principle, this attenuation generates an error that has to be taken into account in the measured ratio I_e/I_t,filtered in Eq. (17), which implies an error in the value of κ. At present, since the attenuation is smaller than 0.1%, this error can be neglected compared to the others uncertainties in κ.

D. Cavity-free spectral range

The dedicated experimental setup for the measurement of the cavity free spectral range $\Delta^{\mathrm{FSR}} = c/2nL_c$ is shown in Fig. 7. The principle is to inject into the cavity two laser beams that are shifted relative to each other by a given frequency. This frequency is then adjusted to coincide with the free spectral range.

Experimentally, the main beam is divided into two parts due to a polarizing beam splitting cube. The first part is directly injected into the cavity and the other one is frequency shifted by the acousto-optic modulator AOM2 with a double-pass configuration before injection. The main beam is frequency modulated with a voltage ramp applied on a piezoelement mounted on the crystal resonator of the laser.

The intensity transmitted by the cavity is observed on Ph$_t$ as shown in Fig. 8. The solid line corresponds to the intensity of the first beam. We observe typical Fabry-Pérot peaks whose frequency gap corresponds to Δ^{FSR}. Peaks due to the second beam (dashed line) are frequency shifted by $2f_{\mathrm{AOM2}}$. We finally adjust f_{AOM2} in order to superimpose both series of peaks. The precise knowledge of the driven frequency f_{AOM2} enables us to

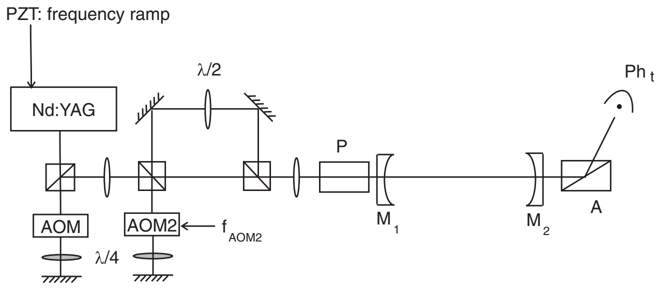

FIG. 7. Experimental setup for the cavity length measurement. Two laser beams that are frequency shifted relative to each other by the AOM2 are injected into the cavity. The frequency of the laser is frequency modulated with a voltage ramp applied on a piezoelement (PZT) mounted on the crystal resonator of the laser. Photodiode Ph_t allows us to observe the typical Fabry-Pérot peaks from which the Δ^{FSR} measurement is performed.

determine with the same precision the value of the free spectral range and thus the cavity length.

A typical value is $\Delta^{\mathrm{FSR}} = (65.996 \pm 0.017)$ MHz. This corresponds to a cavity length of $L_c = (2.2713 \pm 0.0006)$ m. Since this length can be prone to variation, the Δ^{FSR} value is regularly checked and updated.

E. Effective magnetic length

Following Eq. (5), the effective magnetic length L_B has been calculated by numerically integrating the field measured with a calibrated pickup coil. Taking into account the experimental uncertainties, for one X-coil we obtain $L_B = (0.137 \pm 0.003)$ m, which corresponds to a relative type-B uncertainty of L_B of 2.2%.

F. Laser wavelength

As mentioned above, infrared light enters the cavity. The wavelength of the Nd:YAG laser is 1064 nm and its uncertainty is given by the width of the laser transition. The natural linewidth of Nd:YAG lasers is not usually given by the manufacturers. However, we can estimate it from the bandwidth of the gain curve of the amplifying medium. It is typically of the order of 30 GHz [29]. This corresponds to an uncertainty on the laser wavelength of 0.3 nm. In order to be conservative, we use $\lambda = (1064.0 \pm 0.5)$ nm. The relative uncertainty is negligible in our case, compared to main uncertainties.

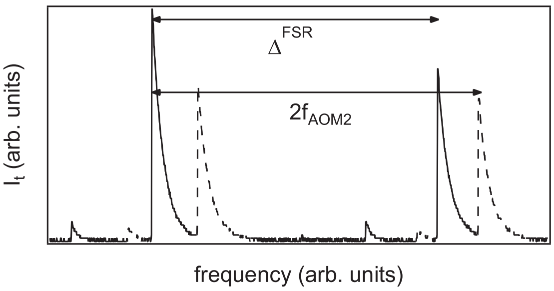

FIG. 8. Transmission peaks of the Fabry-Pérot cavity as a function of the laser frequency. Two beams are sent to the interferometer: The second beam (dashed line) is frequency shifted by $2 f_{\mathrm{AOM2}}$ relative to the first beam (solid line). The adjustment of f_{AOM2} in order to superimpose both series of peaks allows us to precisely measure the free spectral range Δ^{FSR} of the cavity.

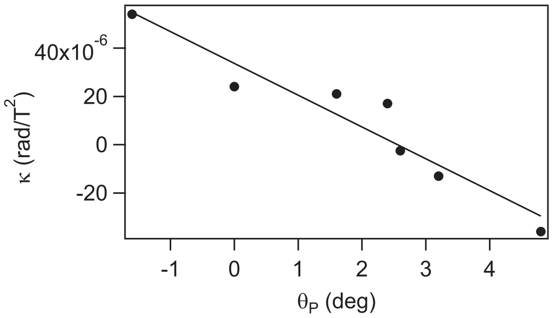

FIG. 9. Correlation factor κ between the square of the magnetic field and the ellipticity as a function of the angle θ_P of the incident polarization.

G. Angle between the incident polarization and the magnetic-field direction

The angle between the incident light polarization and the magnetic-field direction is adjusted to 45° as a result of magnetic birefringence measurements as a function of the polarizer direction θ_P. In order to be more sensitive, this is performed close to the position where the magnetic field is parallel to the polarizer P ($\theta = 0^\circ$).

Measurements are realized with about 7×10^{-3} atm of air. The analyzer direction is crossed at maximum extinction each time the polarizer is turned. Figure 9 represents the evolution of the correlation factor κ as a function of θ_P. Data are fitted by a sinusoidal trend $\kappa(\theta_P) = \kappa_0 \sin[2(\theta_P - \theta_0)]$ giving $\theta_0 = (2.6 \pm 0.2)^\circ$. This measurement allows us to set $\theta = (45.0 \pm 1.2)^\circ$. The uncertainty is mainly due to the mechanical system that holds and turns the polarizer.

H. Error budget

We summarize in Table II the typical values of the experimental parameters that have to be measured and their type-B associated uncertainty. These uncertainties are quadratically added to give a type-B relative uncertainty of the birefringence Δn of 3.1% at 1σ.

TABLE II. Parameters that have to be measured to infer the value of the birefringence Δn and their respective relative type-B uncertainty at 1σ.

Parameter	Typical value	Relative type-B uncertainty
κ	10^{-5} rad T^{-2}	2.2×10^{-2}
Δ^{FSR}	65.996 MHz	3×10^{-4}
L_B	0.137 m	2.2×10^{-2}
λ	1064.0 nm	$<5 \times 10^{-4}$
$\sin 2\theta$	1.0000	9×10^{-4}
	Total	3.1×10^{-2}

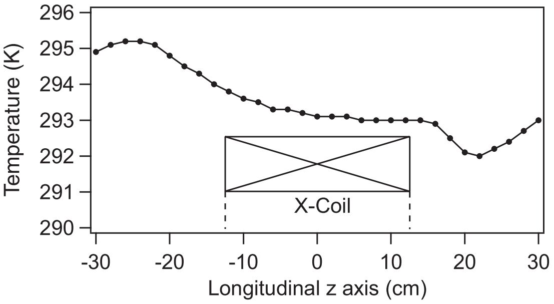

FIG. 10. Profile of the temperature inside the vacuum pipe along the longitudinal $z$axis. The X-coil is also schematized at the center. The temperature variation does not exceed 1 K inside the tube that runs through it.

I. Temperature and pressure of gases

Gas magnetic birefringence measurements are performed at room temperature $T = 293$ K. The experimental room is air conditioned. A flow of compressed air between the outer wall of the vacuum pipe and the liquid-nitrogen cryostat containing the magnet maintains the room temperature in the gas chamber.

A temperature profile has been realized along the length of the vacuum pipe and is plotted in Fig. 10. The temperature variation does not exceed 1 K inside the tube that passes through the magnetic field. Concerning gases, we consider that our birefringence measurements are given at (293±1) K. The pressure of the gas inside the chamber is measured at each side of the vacuum pipe getting into magnets with pressure gauges. The relative uncertainty provided by the manufacturer is 0.2%.

IV. MAGNETIC BIREFRINGENCE MEASUREMENTS

A. Raw signals

Figure 11 presents signals obtained with 32.1×10^{-3} atm of molecular nitrogen. The intensity of the ordinary beam I_t (top) remains almost constant while the intensity of the extraordinary beam I_e (middle) varies when the magnetic field (bottom) is applied. The magnetic field reaches its maximum of 5.2 T within less than 2 ms.

The laser beam remains locked to the Fabry-Pérot cavity, despite mechanical vibrations caused by the shot of magnetic field. The intensities I_t and I_e start oscillating after about 4 ms. Seismometers placed on mirror mounts show that these oscillations are mainly due to acoustic perturbations produced by the magnet pulse and propagating from the magnet to the mirror mounts through the air. We also see that the minimum of I_e does not coincide with the maximum of B^2. This phenomenon is due to the cavity filtering, as explained in detail in Ref. [26].

In Fig. 12 we plot the square of the magnetic field filtered by the cavity and the ellipticity calculated with Eq. (17) as a function of time. Since the acoustic perturbations affect both signals I_t and I_e, by taking into account the cavity filtering between I_t and I_e, oscillations on Ψ are strongly reduced to a few 10^{-5} rad and thus are not visible in this figure. These oscillations induce uncertainty to the measurement, but are already included in the type-A uncertainty on κ measured in Sec. III B.

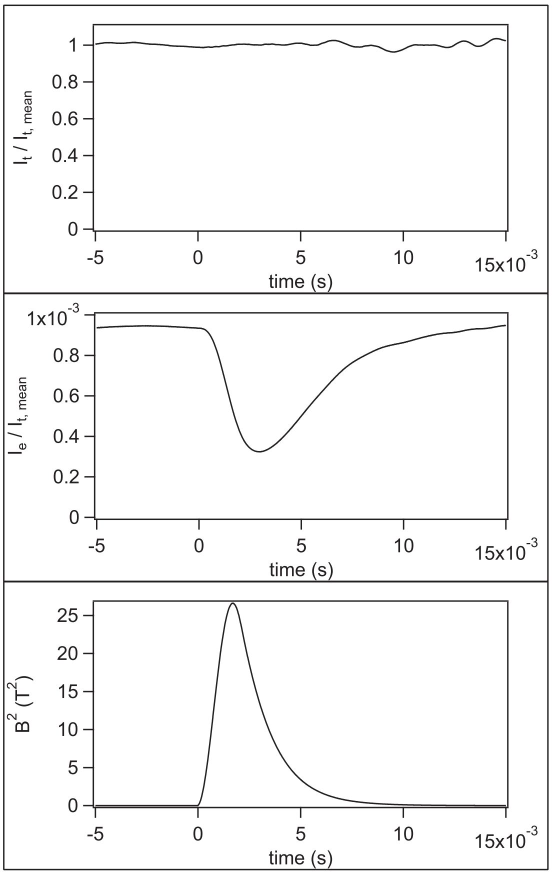

FIG. 11. Cotton-Mouton effect measurements on 32.1×10^{-3} atm of molecular nitrogen: top, normalized intensity of the ordinary beam as a function of time; middle, intensity of the extraordinary beam divided by the mean of I_t as a function of time; and bottom, square of the magnetic field as a function of time.

Finally, we note that both quantities B^2_{filtered} and Ψ reach their extremum at the same time and their variation can be perfectly superimposed, thus providing a precise measurement of magnetic linear birefringence of nitrogen gas.

B. Apparatus calibration

In order to calibrate our apparatus and to evaluate its present sensitivity we have measured the magnetic birefringence of

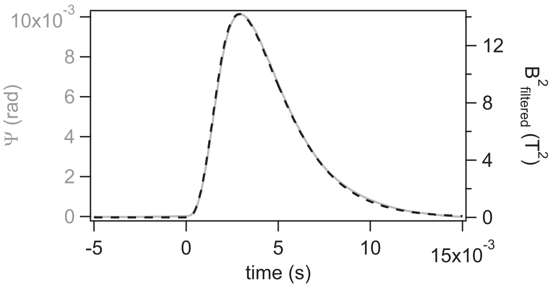

FIG. 12. Cotton-Mouton effect measurement on 32.1×10^{-3} atm of molecular nitrogen. The gray line denotes the total ellipticity as a function of time and the dashed line denotes the square of the magnetic field filtered by a first-order low-pass filter corresponding to the cavity filtering.

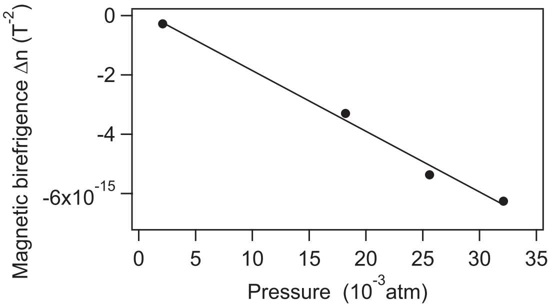

FIG. 13. Magnetic birefringence of molecular nitrogen as a function of pressure. The solid line corresponds to the linear fit of the experimental data.

molecular nitrogen. These measurements have been performed at different pressures from 2.1×10^{-3} to 32.1×10^{-3} atm and are summarized in Fig. 13. In this range, nitrogen can be considered as an ideal gas and the pressure dependence of its birefringence is thus linear:

$$\Delta n[\mathrm{T}^{-2}] = \Delta n_u[\mathrm{atm}^{-1}\,\mathrm{T}^{-2}]P[\mathrm{atm}]. \quad (27)$$

We have checked that our data are correctly fitted by a linear equation. Its Δn axis intercept is consistent with zero within the uncertainties. Its slope gives the normalized magnetic birefringence at $B = 1$ T and $P = 1$ atm (in atm^{-1} T^{-2}):

$$\Delta n_u = (-2.00 \pm 0.08 \pm 0.06) \times 10^{-13}.$$

The first uncertainty 0.08×10^{-13} atm^{-1}T^{-2} corresponds to the fitting uncertainty and represents the type-A total uncertainty at 1σ; the second one 0.06×10^{-13} atm^{-1}T^{-2} represents the type-B uncertainty at 1σ.

Our value of the normalized birefringence is compared in Table III to other published experimental values at $\lambda = 1064$ nm [30,31]. The table shows that our value agrees perfectly well with other existing measurements. Our total uncertainty is 10^{-14} atm^{-1} T^{-2}, calculated by quadratically adding the type-A and type-B uncertainties. This is 1.8 times more precise than the other results. It therefore provides a successful calibration of the whole apparatus.

C. Upper limit on vacuum magnetic birefringence measurements

Once the calibration had been performed we evaluated the upper limit of the present apparatus on vacuum magnetic birefringence. To this end, several pulses were performed in vacuum. A typical ellipticity measured during a magnetic pulse is plotted in Fig. 14. Acoustic perturbations induce oscillations of Ψ starting at about 4 ms, with variations of the order of 10^{-5} rad. In order to infer our best upper limit for the value of the vacuum magnetic birefringence, we limit the integration time to 4 ms. We get $\Delta n < 5.0 \times 10^{-20}$ T^{-2} per pulse.

TABLE III. Comparison between our value of the nitrogen normalized magnetic birefringence and other experimental published values at $\lambda = 1064$ nm.

Ref.	$\Delta n_u \times 10^{-13}$ (at $P = 1$ atm and $B = 1$ T)
[30]	-2.17 ± 0.21
[31]	$-2.02 \pm 0.16 \pm 0.08$
this work	$-2.00 \pm 0.08 \pm 0.06$

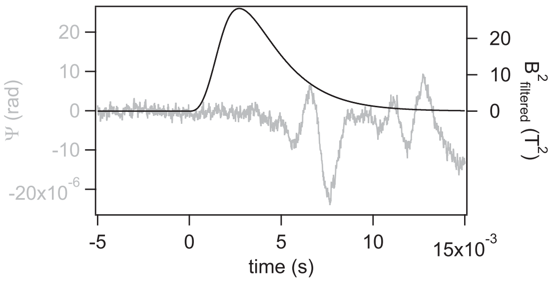

FIG. 14. Typical ellipticity (gray) measured during a magnetic pulse (black) performed in vacuum. Acoustic perturbations generate ellipticity oscillations starting at 4 ms.

During operation, the pressure inside the UHV system was better than 10^{-10} atm. To be conservative, let us assume that residual gases are mainly 78% nitrogen and 21% oxygen. The normalized magnetic birefringences of these gases are of the order of -2×10^{-13} and -2×10^{-12} atm^{-1} T^{-2}, respectively [12]. The total residual magnetic birefringence is then of the order of 6×10^{-23} T^{-2}, which is well below our current upper limit. In the final setup, vacuum quality will be monitored with a residual gas analyzer.

V. CONCLUSION

The successful calibration we report in this paper is a crucial step toward the measurement of vacuum magnetic birefringence. It shows our capability to couple intense magnetic fields with one of the sharpest Fabry-Pérot cavities in the world. It is worthwhile to note that an energy of about 100 kJ is discharged in our coils during a few milliseconds. These 10 MW of electrical power generate acoustic perturbations and mechanical vibrations that tend to misalign the cavity mirrors. The linewidth $\Delta\nu$ of our Fabry-Pérot cavity is of the order of 150 Hz. A relative displacement $\Delta L_c = L_c\Delta\nu/\nu_{\mathrm{laser}} = 1$ pm of both mirrors is enough to get out of resonance. The sharper the cavity, the bigger the challenge.

The sensitivity per pulse we got in both gases and vacuum is outstanding. For the sake of comparison, the best birefringence limit obtained in vacuum with continuous magnets is $\Delta n \leqslant 2.1 \times 10^{-20}$ T^{-2} with an integration time of $t_{\mathrm{int}} = 65\,200$ s [11]. In order to compare both methods, we need to translate the best limit obtained in the continuous regime to the one obtained with our integration time $T_i = 4$ ms. Assuming white noise for both methods, the best limit reported in Ref. [11] corresponds to $\Delta n(T_i) = \Delta n(t_{\mathrm{int}})\sqrt{t_{\mathrm{int}}/T_i} \leqslant 8.5 \times 10^{-17}$ in 4 ms of integration. This value is more than three orders of magnitude higher than ours, proving that pulsed fields are a powerful tool for magnetic birefringence measurements.

The long-term prospective is to get a value of $\Delta n = 4 \times 10^{-24}$ T^{-2}, corresponding to the vacuum magnetic birefringence, with at most 1000 pulses. This corresponds to a sensitivity better than 1.3×10^{-22} T^{-2} per pulse. A factor of the order of 10 of optical sensitivity will be achievable with better acoustic insulation and a more robust locking system, in particular reducing the noise of the measured light intensities transmitted by the cavity. Further improvements depend on the possibility of having higher magnetic fields. We have designed a pulsed coil, called the XXL-coil, which has already reached a field higher than 30 T when a current higher than 27 000 A is injected. This corresponds to more than 300 T^2 m [32]. Two XXL-coils will allow us to improve our current sensitivity by a factor 100. We plan to modify the apparatus in order to host these XXL-coils. Therefore, the final version of the experiment will be ready for operation.

ACKNOWLEDGMENTS

We thank all the members of the Biréfringence Magnétique du Vide collaboration, in particular J. Béard, J. Billette, P. Frings, J. Mauchain, M. Nardone, L. Recoules, and G. Rikken for strong support. We are also indebted to the whole technical staff of LNCMI. We acknowledge the support of the Fondation pour la Recherche IXCORE and the ANR-Programme non Thématique (Grant No. ANR-BLAN06-3-139634).

---

[1] J. Kerr, Br. Assoc. Rep. 568 (1901).
[2] Q. Majorana, Rendic. Accad. Lincei **11**, 374 (1902); C. R. Hebd. Séanc. Acad. Sci. Paris **135**, 159 (1902).
[3] A. Cotton and H. Mouton, C. R. Hebd. Séanc. Acad. Sci. Paris **141**, 317 (1905); **142**, 203 (1906); **145**, 229 (1907); Ann. Chem. Phys. **11**, 145 (1907).
[4] Z. Bialynicka-Birula and I. Bialynicki-Birula, Phys. Rev. D **2**, 2341 (1970).
[5] S. L. Adler, Ann. Phys. (NY) **67**, 599 (1971).
[6] H. Euler and B. Kochel, Naturwissenschaften **23**, 246 (1935).
[7] W. Heisenberg and H. Euler, Z. Phys. **38**, 714 (1936).
[8] V. I. Ritus, Sov. Phys. JETP **42**, 774 (1975).
[9] [http://www.codata.org].
[10] S.-J. Chen, H.-H. Mei, and W.-T. Ni, Mod. Phys. Lett. A **22**, 2815 (2007).
[11] E. Zavattini *et al.*, Phys. Rev. D **77**, 032006 (2008).
[12] C. Rizzo, A. Rizzo, and D. M. Bishop, Int. Rev. Phys. Chem. **16**, 81 (1997).
[13] A. D. Buckingham, W. H. Prichard, and D. H. Whiffen, Trans. Faraday Soc. **63**, 1057 (1967).
[14] R. Cameron *et al.*, Phys. Rev. D **47**, 3707 (1993).
[15] C. Rizzo, Europhys. Lett. **41**, 483 (1998).
[16] R. Battesti *et al.*, Eur. Phys. J. D **46**, 323 (2008).
[17] R. W. P. Drever, J. L. Hall, F. V. Kowalski, J. Hough, G. M. Ford, A. J. Munley, and H. Ward, Appl. Phys. B **31**, 97 (1983).
[18] S. Batut *et al.*, IEEE Trans. Appl. Supercond. **18**, 600 (2008).
[19] F. Brandi, F. Della Valle, A. M. De Riva, P. Micossi, F. Perrone, C. Rizzo, G. Ruoso, and G. Zavattini, Appl. Phys. B **65**, 351 (1997).
[20] O. Svelto, *Principles of Lasers*, 4th ed. (Springer, Berlin, 1998), pp. 167–168.
[21] Virgo Collaboration, Appl. Opt. **46**, 3466 (2007).
[22] G. Heinzel, Class. Quantum Grav. **18**, 4113 (2001).
[23] M. Rakhmanov *et al.*, Class. Quantum Grav. **21**, S487 (2004).
[24] D. Jacob, M. Vallet, F. Bretenaker, A. Le Floch, and M. Oger, Opt. Lett. **20**, 671 (1995).
[25] F. Bielsa, A. Dupays, M. Fouché, R. Battesti, C. Robilliard, and C. Rizzo, Appl. Phys. B **97**, 457 (2009).
[26] P. Berceau, M. Fouché, R. Battesti, F. Bielsa, J. Mauchain, and C. Rizzo, Appl. Phys. B **100**, 803 (2010).
[27] Figures 3 and 4 do not correspond to the same run of data and thus cannot be directly compared.
[28] P. J. Mohr and B. N. Taylor, J. Phys. Chem. Ref. Data **28**, 1713 (1999).
[29] J. Hecht, *The Laser Guidebook*, 2nd ed. (McGraw-Hill, New York, 1992), p. 403.
[30] M. Bregant *et al.*, Chem. Phys. Lett. **392**, 276 (2004).
[31] H.-H. Mei, W.-T. Ni, S.-J. Chen, and S.-S. Pan, Chem. Phys. Lett. **471**, 216 (2009).
[32] [http://www.toulouse.lncmi.cnrs.fr/spip.php?rubrique32].